JOURNAL OF Applied Polymer SCIENCE

Fullerene Containing Polyurethane Nanocomposites for Microwave Applications

Swati Chopra, Sarfaraz Alam
Defence Materials Stores Research and Development Establishment, Kanpur - 208 013, Uttar Pradesh, India
Correspondence to: S. Alam (E-mail: sarfarazkazmi@yahoo.com)

ABSTRACT: Novel flexible polyurethane (PU) composite films containing nano-barium hexaferrite (BaF) and nano-barium titanate (BT) have been synthesized and characterized. The PU nanocomposites were synthesized from fullerenol and prepolymer of hexamethylene diisocyante and polytetramethylene glycol by adding 1–3% each of BaF (high permeability) and BT (high permittivity). The incorporation of the nanopowders was confirmed by X-ray diffraction (XRD), transmission electron microscopy, and energy dispersive X-ray diffraction (EDX). Study of thermal properties by thermogravimetric analysis and dynamic mechanical analysis revealed enhanced thermal stability of the nanocomposites. Study of mechanical properties showed that the tensile strength had increased remarkably in the nanocomposites. The electromagnetic-absorbing properties were studied by measuring the complex permeability and permittivity in the frequency range of 8.2 to 12.4 GHz. The good reflection loss of the nanocomposites at such low filler content suggests its potential applicability as a radar absorber. © 2012 Wiley Periodicals, Inc. J. Appl. Polym. Sci. 000: 000–000, 2012

KEYWORDS: polyurethanes; fullerenes; nanocomposites; transmission electron microscopy

Received 25 May 2011; accepted 11 July 2012; published online
DOI: 10.1002/app.38343

INTRODUCTION

Shielding against electromagnetic (EM) radiation has drawn more attention recently due to the increasing use of gigahertz (GHz) EM waves in commercial, military, scientific, electronic, and communication systems. Microwave absorbers have been used since long to minimize EM reflection from structures such as aircraft, ships, tanks etc due to the fact that they can absorb radiation energy from microwave generated from an electric source. In general, EM wave absorption characteristics of a material depend on their complex permittivity ($\varepsilon_r = \varepsilon' - j\varepsilon''$), complex permeability ($\mu_r = \mu' - j\mu''$), EM impedance match, and microstructure of the absorber.[1–3]

Barium Titanate $BaTiO_3$ (BT) is one such ferroelectric material exhibiting high dielectric constant. Extensive research has been conducted on the synthesis, morphology, ferroelectricity, and permittivity properties of BT.[4,5] The characteristic feature of BT is that the Ba^{2+} and O^{2-} ions form a face centered cubic (fcc) lattice with Ba^{2+} at the corners and O^{2-} at the face centers. The Ti^{4+} ions sit in the octahedral interstices formed by six O^{2-} ions. At room temperature, there is possibly minimum energy position for the Ti^{4+} ion, which is off-centered and therefore gives rise to permanent electric dipoles formed with six O^{2-}. Studies on EM wave absorbers of BT and its complex materials are of current interest; however, its low permeability limits its microwave-absorbing character.[6–8]

In recent years, hexagonal ferrites like barium hexaferrite $BaFe_{12}O_{19}$ (BaF) have displayed a promising application as a radar-absorbing material[9,10] in the GHz range where spinel ferrites do not work well due to a drop in the complex permeability as given by snoek's limit.[11] Nanosized hexagonal BaF has a single magnetic domain, because of which it has excellent magnetic properties[12] and it also helps reduce eddy current losses.[13] Its large magnetization and magnetocrystalline anisotropy, high stability, excellent frequency response, unusually large coercivity[14–16] make it a potential good magnetic loss material in high frequency band,[17,18] but its poor dielectric loss confines its application.

For attaining good microwave absorption, composite materials with lossy fillers (dielectric/magnetic) into the polymer matrix that does not absorb in microwave region have long been the focus of attention. The fabrication of such ceramic-polymer nanocomposites combines the low temperature processing of polymers and the high dielectric/magnetic properties of the nanofillers.[19–21] A review on polymeric nanocomposites for EM wave absorption by Huo et al.[22] summarizes the approach to design the ideal absorber and covers a range of polymeric hosts and several dielectric and magnetic materials contributing to EM absorption. Studies on effect of nano-BT/nano-BaF incorporation into poly(ether ether ketone)/polyurethane (PU) composites have been performed by our group.[23–26]

Keeping this in view, in the present communication, the effect of two lossy fillers, BT for its dielectric and barium ferrite for its magnetic contribution have been investigated on PU matrix by varying each of their concentration from 1–3%. The free-standing flexible PU films have been synthesized in our laboratory from fullerenol (hydroxyl fullerene) as a hypercrosslinker.[27] Fullerenol was preferred as a crosslinker owing to its several reactive exo hydroxy groups, which would facilitate the formation of a three-dimensional crosslinked network with enhanced mechanical properties.[28] Also, fullerene-derived PU elastomers based actuators are reported to operate at low voltage.[29] Hence, fullerenol was incorporated with a primary objective to improve mechanical properties and owing to its dielectric nature was expected to improve microwave absorption too.

EXPERIMENTAL

Materials

Fullerene C_{60} (CMer, 99.9%), hexamethylene diisocyanate (Acros) (HDI), Dibutyltin dilaurate (Aldrich) (DBTDL), nano-$BaFe_{12}O_{19}$ (BaF), nano-BT, and Triton-X114 were procured from Sigma Aldrich. Polytetramethylene glycol (PTMG) (M_w = 2000) was dried in vacuum for 2 days to ensure complete removal of moisture. Methanol, dimethyl formamide (DMF), and tetrahydrofuran (THF) have been dried by known methods[30] and stored over molecular sieves (4 Å) before use.

Synthesis of BaF and BT Incorporated Fullerene Containing PU Flexible Freestanding Nanocomposite Film (B-PU)

Synthesis of PU nanocomposite has been performed by first preparing prepolymer and then incorporating nanofillers (BT and BaF) and crosslinker (fullerenol) to form highly crosslinked PU film.

Synthesis of Fullerenol and Prepolymer of PTMG and HDI. Fullerenol containing 12–13 hydroxy groups was synthesized by Chiang et al. method.[31] PTMG and HDI (NCO index 4) were stirred in a three-necked round bottom flask at 70°C for 2 h in an inert atmosphere and synthesis of prepolymer was confirmed by the appearance of urethanic carbonyl at 1720 cm^{-1} and suppression in 2200 cm^{-1} peak intensity due to isocyante linkages, in the infrared (IR) spectrum.[27]

Synthesis of B-PU Nanocomposite. In a separate round bottom flask, variable concentrations of BT and BaF (0.01 weight % TritonX as dispersant) were sonicated in THF and added to the three-necked flask containing prepolymer (synthesized as above) with vigorous stirring. Fullerenol, dispersed in anhydrous mixture of THF and DMF (3 : 1), was added to the above reaction mixture along with a dilute drop of DBTDL catalyst. The temperature was raised to 60°C and inert atmosphere was maintained throughout the reaction. The reaction viscosity began to increase, as expected by the crosslinking effect of fullerenol, and at an appropriate viscosity, that is just before turning into a gel, the contents of the flask were poured onto a glass plate or petridish and left overnight to obtain flexible freestanding B-PU nanocomposite films (Scheme 1).

Characterization

Fourier transform IR (FTIR) spectra were recorded on a Nicolet Magna IR 750 spectrometer, using KBr pellets. Thermogravimetric measurements were performed by a Hi-Res TGA 2950 thermogravimetric Analyzer (TA instruments) attached to a thermal analyst 2100 (DuPont Instruments) thermal analyzer, under nitrogen from room temperature to 600°C, with a heating rate of 10°C/min. About 7 ± 0.2 mg of sample was heated at 10°C/min for comparative thermogravimetric analysis (TGA). Dynamic mechanical analysis (DMA) was performed by GABO EXPLEXOR 150 N at a heating rate of 2°C/min from −100°C to −20°C. X-ray diffractograms (XRD) were acquired at room temperature on an ARL XTRA X-ray diffractometer (Thermo Electron Corporation) with Cu Kα radiation in the 2θ range from 10 to 80°, by a step of 0.02°. Energy dispersive X-ray spectrogram (EDX) was recorded on Genesis 1000 attached with Carl Zeiss Scanning Electron Microscope. The size and morphology of fillers used in the composite were confirmed by Technai G^2 U-Twin High Resolution Transmission electron microscope and EDX of the nanocomposite was recorded on EDX attached with TEM instrument. Sintech Universal Mechanical Testing Unit was used to measure the tensile properties of polymers. All the given values are means of six measurements (± standard deviation). The standard dumb-bell shaped samples (ASTM D638) were used in measurement with a constant stretching rate of 50 mm/min ± 10. Agilent PNA Series vector network analyzer E8364B (110–50 MHz) at X band (8.2–12.4 GHz) of microwave region was used to determine the real and

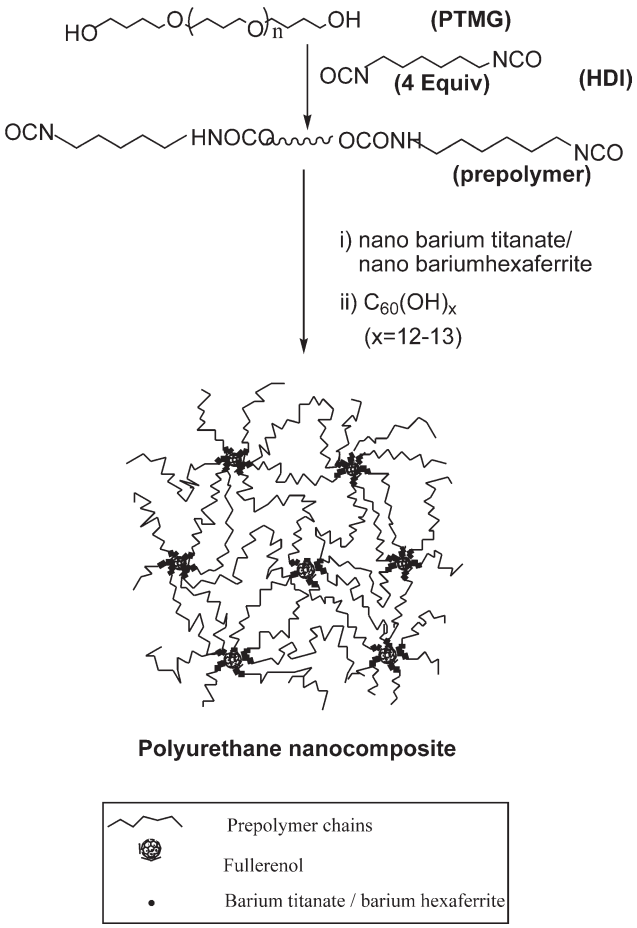

Scheme 1. Schematic of synthesis of nanocomposite.

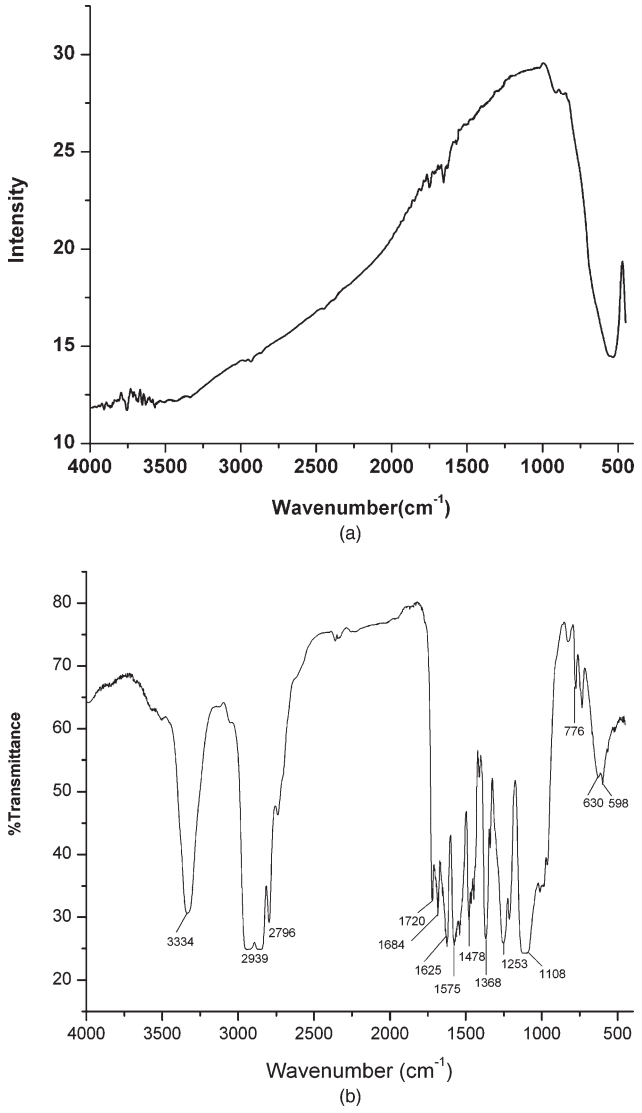

Figure 1. IR spectra of (a) BT (b) B-PU nanocomposite.

imaginary permittivity (ε', ε'', μ', μ''). The values were measured by Agilent X-Band (WR-90) waveguide kit using the material measurement software 85701.

RESULTS AND DISCUSSION

FTIR Spectrum

The FTIR spectrum of BT is shown in Figure 1(a). Figure shows absorption between 580 and 460 cm^{-1}, which are characteristic stretching (str) of Ti—O bonds. [4] In Figure 1(b), which shows IR spectrum of B-PU nanocomposite, the bands at 3334 and 1478 cm^{-1} can be attributed to N—H str, while the urethanic carbonyl is evident at 1720 cm^{-1}. The broad bands at 2900–2800 cm^{-1} can be accounted to C—H str, at 1108 to C—O—C str, while at around 1625 to C=C str, respectively. Hence, the synthesis of PU is clearly evidenced by IR. However, as the characteristic bands of BT and BaF are found between 550 and 400 cm^{-1}[26,32] and these bands are already present in the fullerene-derived PU, nanofiller incorporation can not be affirmed by IR. Following analytical techniques have been used to prove the nanocomposite formation.

X-Ray Diffraction (XRD)

Figure 2(a,b) plot the XRD diffractograms of BT and B-PU nanocomposite, respectively. The XRD spectrum in Figure 2(a) shows cubic symmetry with reflection peaks at 2θ values of 22.32, 31.69, 39.05, 45.49, 51.15, 56.39, and 66.01 corresponding to (100), (110), (111), (200), (210), (211), and (220) sets of diffraction planes, respectively and can be indexed to JCPDS#05-0626 (Joint Committee on Powder Diffraction Standards). The peaks in XRD spectrum of BaF[26] are in accord with the magnetoplumbite structure of hexagonal BaF (JCPDS #84-0757). The average particle size of BaF and BT is estimated from the line broadening of corresponding X-Ray diffraction peaks using the Scherrer formula.[33]

$$d = \frac{0.9l\lambda}{\beta\cos\theta}$$

where, d is the primary particle size, λ is the wavelength of Cu Kα radiation (1.5405 Å), θ is the diffraction angle, and β is the line width at half maximum height. The average particle size of

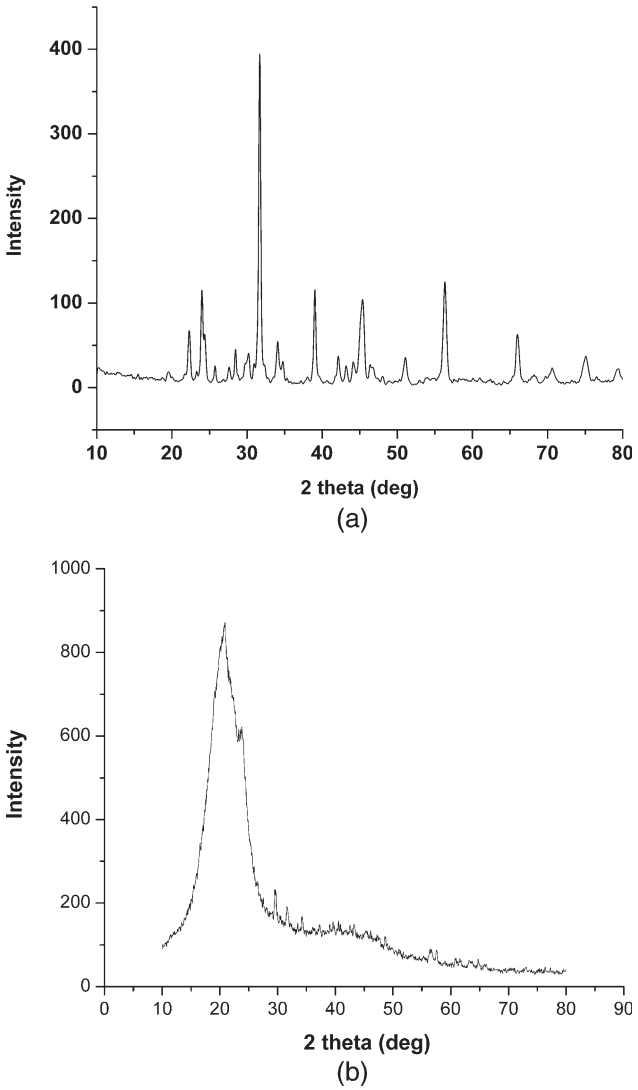

Figure 2. XRD spectra of (a) BT (b) B-PU nanocomposite.

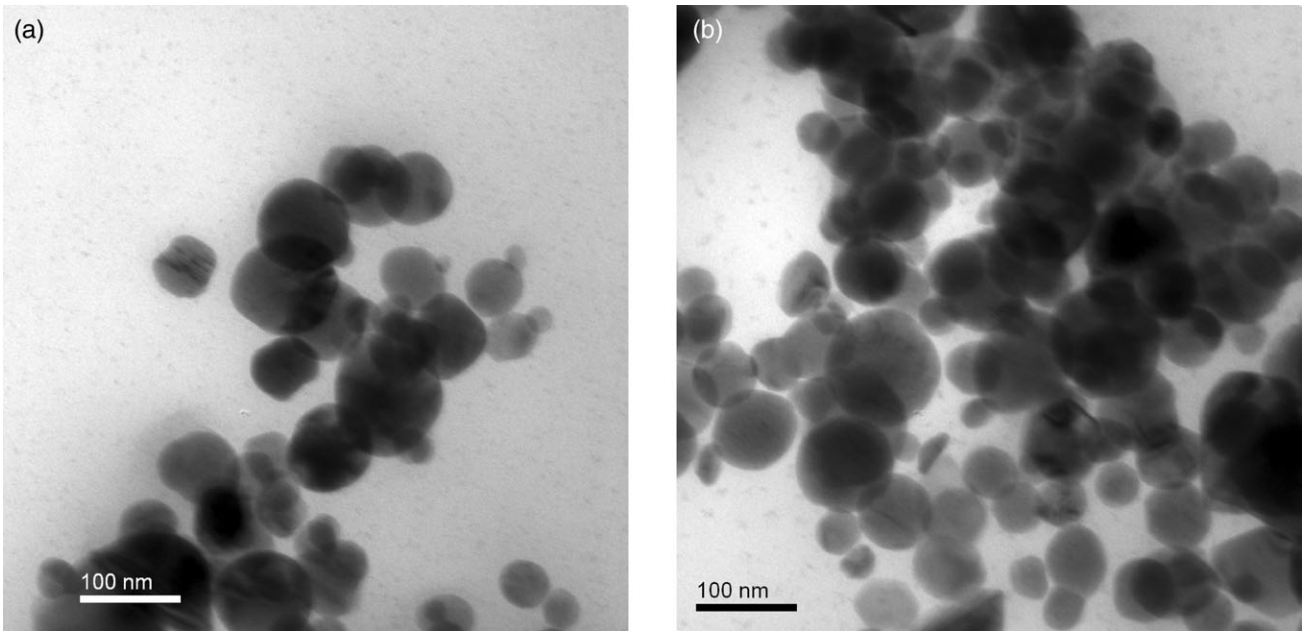

Figure 3. TEM micrograph of (a) BT (b) B-PU nanocomposite.

BaF is calculated to be 49 nm and that of BT to be 65 nm. Figure 2(b) shows a broad peak between 18 and 23 2θ that can be attributed to PU matrix, all sharp peaks at 31.6, 39.07, 45.45, and 57.5 can be attributed to the presence of BT and the peaks at 32.1, 34.2, 37.2, 40.3, and 63.1 can be accounted to BaF. Hence, the XRD spectrum of the nanocomposite clearly proves the incorporation of nanoparticles into the PU matrix.

Transmission Electron Microscopy

Figure 3(a) shows the TEM micrograph of BT nanoparticles. Most of the particles are irregular in the size range of 50–100 nm, with few reaching cubic shape. TEM image of BaF[26] also shows a mixture of spherical and hexagonal particles in the same range. The TEM micrograph of B-PU nanocomposite [Figure 3 (b)] shows that about 80–90% of the particles are ranged from 50 to 100 nm and all shapes, that is, spherical, cubic, and hexagonal are evident suggesting the incorporation of both BT and BaF nanofillers. Agglomeration between hexagonal ferrite particles may be attributed to the magneto dipole attraction and the smaller spherical particles evident in the micrograph are probably of fullerene moiety.

Energy Dispersive X-Ray Diffraction (EDX)

Table I describes the EDX analysis of BT and BaF nanoparticles. Both the atomic and weight % values are in accordance with expected values. Figure 4 shows the EDX spectrum of B-PU nanocomposite. As this spectrum was obtained from carbon coated copper grid, the weight % values cannot be used to quantify the filler incorporation, but the spectrum certainly does provide an evidence for BaF and BT incorporation into PU matrix.

Thermal Properties

Figure 5 shows the TGA thermogram of PU and its nanocomposites. From the plot of percent decomposition versus temperature, it appears that onset of degradation has shifted from approximately 306°C for PU to 320°C for PU-3 showing the enhanced thermal stability of nanocomposite of BT and BaF, over fullerene-derived PU. This increase in stability is more clearly evident from the first derivative curve, which shows peak shift from 417°C for PU to 429°C for PU-3. This improvement in thermal stability with increasing filler concentration may be explained by increased surface area available for interfacial interaction between polymer and nanoparticle. Both the nanoparticles used are oxides and hence are expected to interact by polar bond interaction with the isocyanate and ether groups of PU matrix, resulting into better thermal properties.[34] As the loading of filler increases, so does the interfacial interaction leading to improvement in thermal properties.

The variation in storage modulus (E') and tan δ obtained from the DMA measurements are shown in Figure 6. The variation of E' and tan δ with temperature suggests the existence of two transitions for all the samples (marked as arrows in Figure 6). From the E' plot for PU (i.e., without nanofiller), it is evident that the first drop in modulus (although not significant) occurs at approximately −80°C that corresponds to the glass transition temperature (T_g) of fullerene-derived PU.[28] The next significant drop in modulus occurs at approximately −57°C. Earlier

Table I. EDX Data of BaF and BT

		Weight %	Atomic %
Barium titanate	Ba	62.12	20.5
	Ti	19.05	18.05
	O	21.75	61.37
Barium hexaferrite	Ba	12.91	3.49
	Fe	63.5	41.9
	O	23.59	54.5

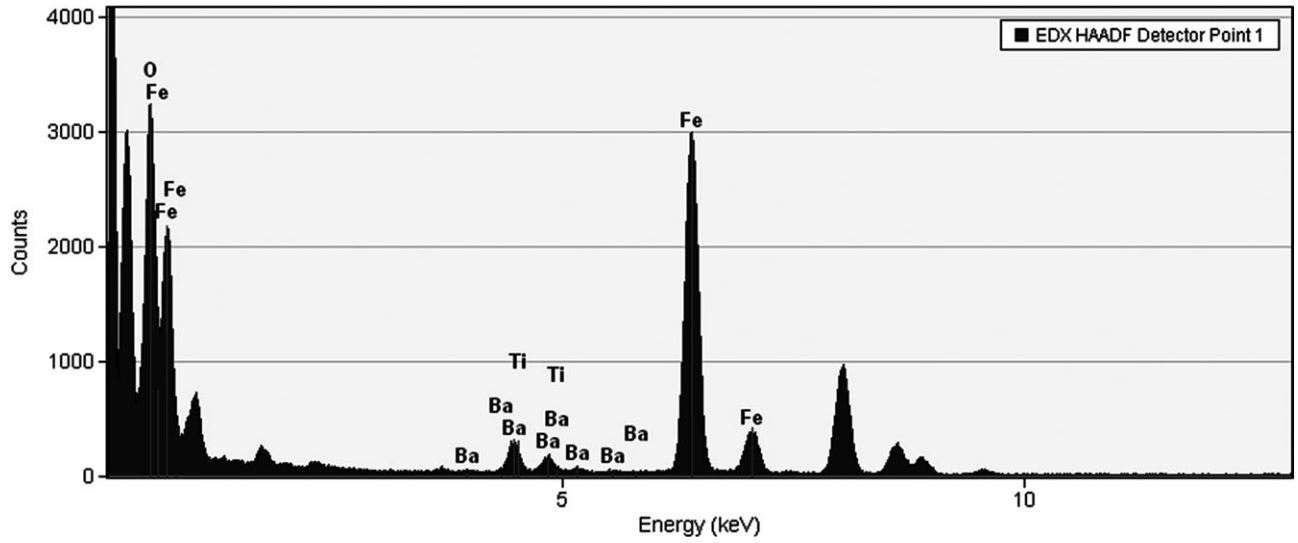

Figure 4. EDX spectrum of B-PU nanocomposite.

differential scanning calorimetry studies on fullerene-derived PU reveal that the flexible polytetramethylene (PTMG) chains have a tendency to recrystallize at approximately −34°C on cooling from melt.[28,35,36] These recrystallized chains are expected to soften beyond T_g. It is hereby proposed that such a softening of the crystalline segments occurs at approximately −57°C which results to the observed drop in E' value. Corresponding to these two transitions, two maxima are also obtained in the tan δ versus temperature plot.

The DMA plots of the nanocomposites (PU-1 to PU-3) also show these two transitions. The plots of storage modulus versus temperature show a decrease with increase in temperature for all the nanocomposites. The first (less significant) transition attributable to T_g does not show significant change compared to PU, whereas the next transition (marked by rapid drop in modulus) is found to shift toward higher temperature as we move from PU-1 to PU-3. It is suggested that with higher loading of filler, the particle–matrix interfacial area increases leading to better interaction. This improved interaction will thereby cause the crystallized PTMG chains to soften at a higher temperature. Hence, the storage modulus drops at a higher temperature compared to PU. This effect could also be interpreted from the tan δ maximum in the region −48 to −36°C.

Mechanical Properties

Table II shows the enhancement in tensile strength with increasing concentration of the filler. The linear PU using butanediol as chain extender in place of fullerenol was also synthesized and found to have a tensile strength of 5 MPa while the fullerene containing PU has tensile strength of 12 MPa.[26] Addition of 1–3% of each nanofiller raises its tensile strength upto 29 MPa ± standard deviation. This significant enhancement in tensile strength with increasing filler content may be explained due to uniform dispersion of filler leading to increased interfacial particle–matrix interaction. The percent elongation was found to decrease with increasing filler concentration. Hence, the

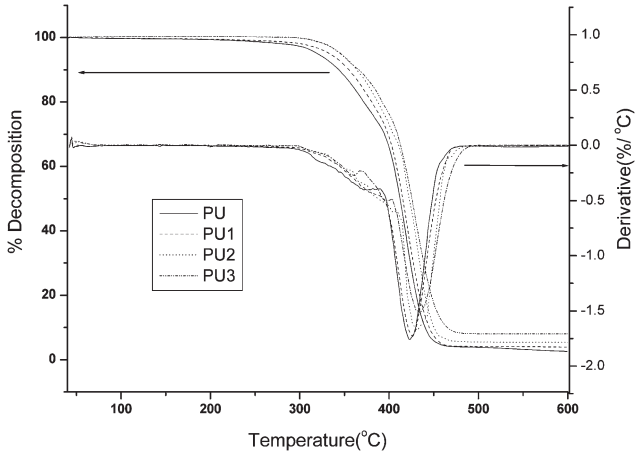

Figure 5. TGA thermograms of PU and 1, 2, and 3% B-PU nanocomposites.

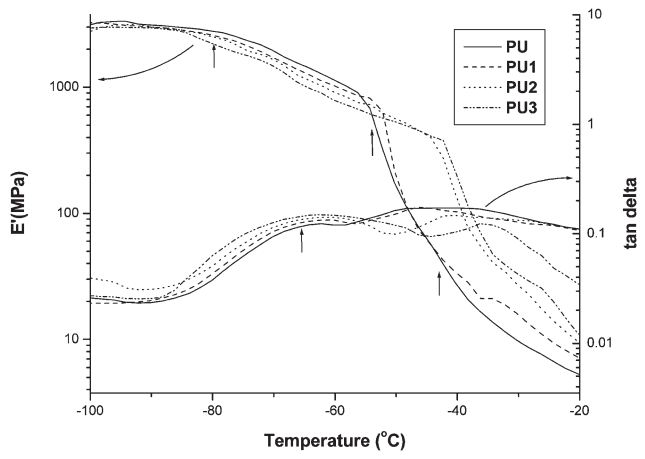

Figure 6. DMA thermograms of PU and 1, 2, and 3% B-PU nanocomposites.

Table II. Tensile Properties of B-PU Nanocomposites

S.Name	% BT	% BaFe	Tensile strength (MPa)	Standard deviation	% Elongation (E_b)
PU	0	0	12.4	2.1	800
PU-1	1	1	13.5	2.2	780
PU-2	2	2	21.1	2.9	670
PU-3	3	3	29.2	3.5	600

nanofiller imparts remarkable mechanical strength to the nanocomposite.

Microwave-Absorbing Properties

Figure 7(a) plots the real (ε') and imaginary (ε'') permittivity versus frequency while Figure 7(b) plots the tan δ_ε curve of PU and its nanocomposites. It is clear from Figure 7(a) that addition of nanofillers raises ε' for PU from approximately 2.3 to a maximum of 4.2. It is also clearly evident from the figure that addition of nanofiller is responsible for a significant increment in ε'', thereby incorporating absorption characteristics to the nanocomposites. This is also evident from sharp rise in tan δ_ε peak of B-PU nanocomposites with 2 and 3% filler content [Figure 7(b)]. The resonance peak rises from 0.08 for PU to 0.29 for PU-3 at 10.3 GHz, which may be due to inherent dielectric property of BT nanoparticles.

Figure 8(a) plots the real (μ') and imaginary (μ'') permeability versus frequency for PU and its nanocomposites. As expected by the dielectric nature of PU, μ' is around 1 and $\mu'' \approx 0$. The nanocomposites show an increase in both μ' and μ'' due to incorporation of BaF. From the tan δ_μ versus frequency plot [Figure 8(b)], it is evident that loss factor (tan δ_μ) is a maximum for 2% BT and 2% BaF composition (PU-2) in the X band region.

For a microwave-absorbing layer backed by a perfect conductor, the normalized input impedence related to the impedence in

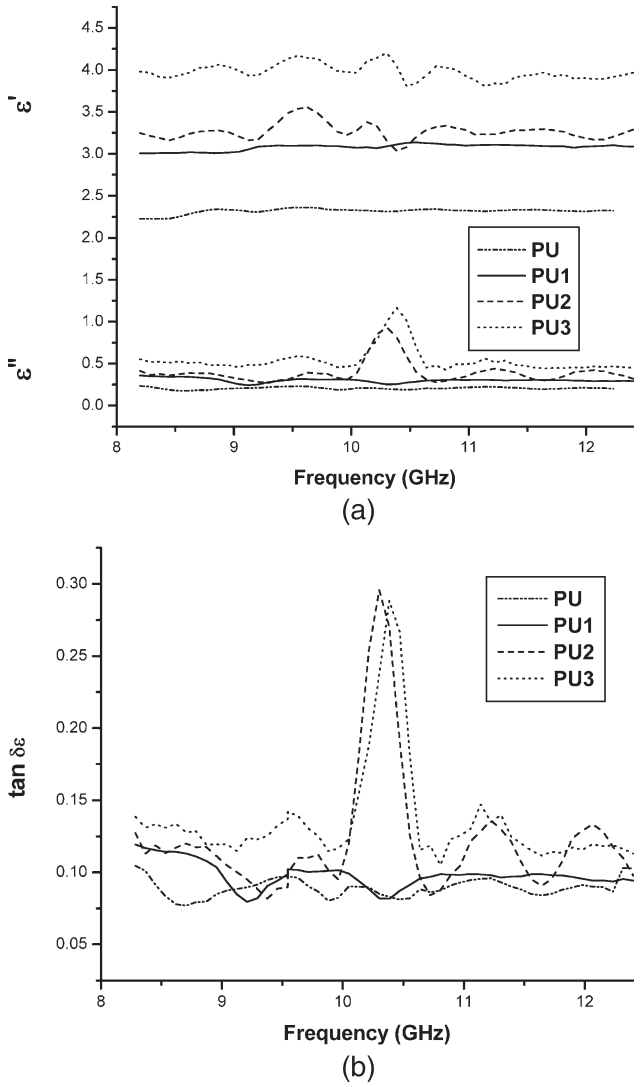

Figure 7. Plot of (a) real (ε') and imaginary (ε'') permittivity versus frequency and (b) tan δ_ε versus frequency of PU and B-PU nanocomposites.

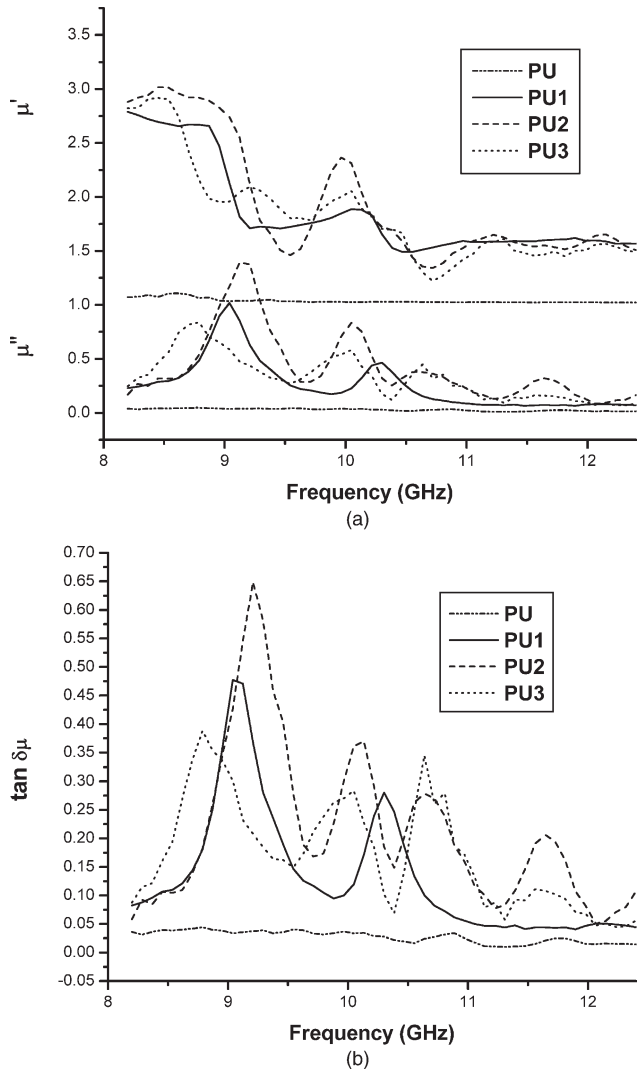

Figure 8. Plot of (a) real (μ') and imaginary (μ'') permeability versus frequency and (b) tan δ_μ versus frequency of PU and B-PU nanocomposites.

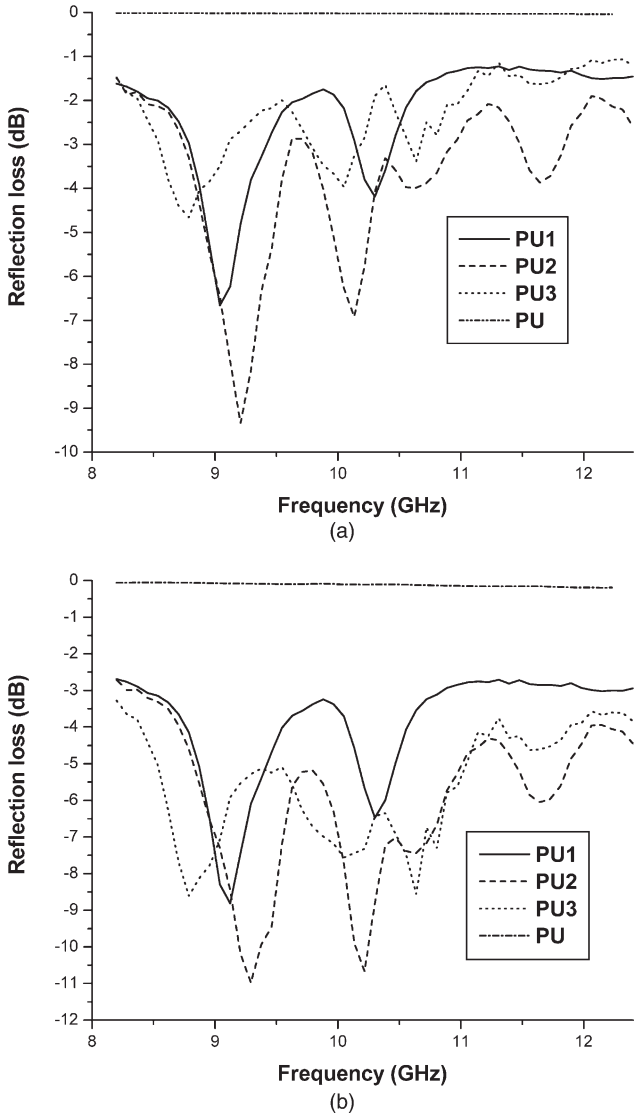

Figure 9. Plot of reflection loss versus frequency of (a) 2 mm (b) 3 mm thickness of PU and B-PU nanocomposites.

free space, Z_{in} and reflection loss (RL) related to the normal incident plane wave are given by the theory of absorbing wall,

$$Z_{in} = \sqrt{\frac{\mu_r}{\varepsilon_r}} \tanh \left[j \frac{2\pi fd}{c} \sqrt{\mu_r \varepsilon_r} \right] \quad (1)$$

$$\mathrm{RL\,(dB)} = 20 \log \left| \frac{Z_{in} - 1}{Z_{in} + 1} \right| \quad (2)$$

where RL is a ratio of reflected power to incident power in dB, ε_r and μ_r are the complex permittivity and complex permeability of the composite medium, respectively, d is the thickness of the absorber, and c and f are the velocity of light and the frequency of microwave in free space, respectively. The impedence matching condition representing perfect absorbing properties is given by $Z_{in} = 1$.

B-PU nanocomposite films having thickness 2 and 3 mm were used for measurement of reflection loss. Figure 9(a,b) shows the reflection losses of PU and B-PU nanocomposites as a function of frequency. It is clear from the figures that PU does not give any reflection loss in the measured frequency band. As shown in Figure 9(b), PU-1 shows a maximum reflection loss of −8.9 dB at 9.1 GHz, PU-2 shows −11 dB at 9.3 GHz and PU-3 shows −8.7 dB at 8.9 GHz. As observed, sample PU-2 shows a maximum absorption in comparison to PU-3. It appears that when doping of BT and BaF is 2% (PU-2), the composites have good compatible dielectric and magnetic properties. As discussed above, for wave to enter into the material there should be good impedance matching at air and material interface. It is quite possible that sample PU-2 exhibits better impedance matching at the interface and therefore gives better absorption. The enhanced microwave properties of B-PU nanocomposite at such low filler content may also be attributed to the nanometer size of the particles, which provide large surface area and increased number of dangling bond atoms and unsaturated coordination on the surface.

CONCLUSIONS

Flexible novel nanocomposite films of fullerene containing PU with BT and BaF as lossy fillers have been prepared and characterized. The effect of incorporating lower content of lossy fillers into PU matrix has been studied by the study of their morphology, mechanical, thermal, and microwave-absorbing properties (X band). The films show enhanced thermal stability and marked improvement in tensile strength. Incorporation of nanofillers enhances the reflection loss of the PU matrix suggesting them potentially applicable as microwave absorbers.

ACKNOWLEDGMENTS

Authors are thankful to DIRECTOR, DMSRDE for providing the technical and financial support under the project DRM-546. Thanks are also due to the Central Analytical Facility, DMSRDE for providing SEM and EDX facility, Strategic Materials Group, DMSRDE for microwave measurements and TEM facility at IIT Kanpur.

REFERENCES

1. Park, K. Y.; Lee, S. E.; Kim, C. G.; Han, J. H. *Compos. Sci. Technol.* **2006,** *66*, 576.
2. Vinoy, K. J.; Jha, R. M. Radar absorbing materials: From theory to design and characterization vol. 1; Kluwer Academic Publishers: Dordrecht (Netherlands), **1996.**
3. Park, K. Y.; Han, J.-H.; Lee, S.-B.; Kun, J.-B.; Yi, J.-W.; Lee, S.-K. *Compos. Sci. Technol.* **2009,** *69*, 1271.
4. Pant, H. C.; Patra, M. K.; Verma, A.; Vadera, S. R.; Kumar, N. *Acta Mater.* **2006,** *54*, 3163.
5. Herbert, J. H. Ceramic Dielectrics and Capacitors; Gordon and Breach: New York, **1985.**
6. Abbas, S. M.; Chandra, M.; Verma, A.; Chatterjee, R.; Goel, T. C. *Compos. Part A* **2006,** *37*, 2148.
7. Wang, G.; Chen, X.; Duan, Y.; Liu, S. *J. Alloys Compd.* **2008,** *454*, 340.
8. Murugan, M.; Kokate, V. K.; Bapat, M. S.; Sapkal, A. M. *Bull. Mater. Sci.* **2010,** *33*, 657.

9. Dishovaski, N.; Petkov, A.; Nedkov, I.; Pazkazov, I. *IEEE Trans. Magn.* **1994,** *30*, 969.
10. Kwon, H. T.; Shin, J. Y.; Oh, J. H. *J. Appl. Phys.* **1994,** *75*, 6109.
11. Ping, X. U.; Han, X.; Wang, M. *J. Phys. Chem. C.* **2007,** *111*, 5866.
12. Kim, M.-H.; Jung, D.-S.; Kang, Y.-C.; Choi, J.-H. *Ceramics Int.* **2009,** *35*, 1933.
13. Kim, D. Y.; Chung, D. C.; Kang, T. W.; Kim, H. C. *IEEE Trans. Magn.* **1996,** *32*, 555.
14. Wohlfarth, E. P. Ferromagnetic Materials; North-Holland: New York, **1982;** Vol. *3*.
15. Jiang, J.; Ai, L.-H.; Qin, D.-B.; Liu, H.; Li, L.-C. *Synth. Met.* **2009,** *159*, 695.
16. Surig, C.; Hempel, K. A.; Bonnenberg, D. *Appl. Phys. Lett.* **1993,** *63*, 2836.
17. Sugimoto, S.; Kondo, S.; Okayama, K. *IEEE Trans. Magn.* **1999,** *35*, 3154.
18. Singh, P.; Babbar, V. K.; Razdan, A.; Srivastava, S. L.; Agarwal, V. K.; Goel, T. C. *J. Mater. Sci.* **2006,** *41*, 7190.
19. Jing, X.; Shen, X.; Song, H.; Song, F. *J. Polym. Res.* **2011,** *18*, 2017.
20. Guo, Z. H.; Park, S.; Hahn, H. T.; Wei, S. Y.; Moldovan, M.; Karki, A. B.; Young, D. P. *J. Appl. Phys.* **2007,** *101*, 09M511.
21. Chen, Y. J.; Cao, M. S.; Wang, T. H.; Wan, Q. *Appl. Phys. Lett.* **2004,** *84*, 3367.
22. Huo, J.; Wang, L.; Yu, H. *J. Mater. Sci.* **2009,** *44*, 3917.
23. Dwivedi, M.; Alam, S.; Verma, G. L. *Polym. Int.* **2005,** *54*, 401.
24. Dwivedi, M.; Alam, S.; Verma, G. L. *J. Therm. Anal. Calorim.* **2005,** *77*, 947.
25. Dwivedi, M.; Alam, S.; Verma, G. L. *Polym. Plast. Technol. Eng.* **2005,** *44*, 1235.
26. Chopra, S.; Pandey, M.; Alam, S. *J. Appl. Polym. Sci.* **2011,** *120*, 3204.
27. Chopra, S.; Mathur, S.; Alam, S. *J. Polym. Mater.* **2008,** *25*, 275.
28. Wang, L.-Y.; Wu, J.-S.; Tseng, S.-M.; Kuo, C.-S.; Hsieh, K.-H.; Liau, W.-B.; Chiang, L.-Y. *J. Polym. Res.* **1996,** *3*, 1.
29. Kyokane, J.; Ishimoto, H.; Yugen, H.; Hira, T.; Ueda, T.; Yoshino, K. *Synth. Met.* **1999,** *103*, 2366.
30. Armarego, W. L. F.; Chai, C. L. L. Purification of Laboratory Chemicals, 5th Ed; Elsevier: MA, USA, **2003.**
31. Chiang, L. Y.; Wang, L.-Y.; Swirczewski, J. W.; Soled, S.; Cameron, S. *J. Org. Chem.* **1994,** *59*, 3960.
32. Waldron, R. D. *Phys. Rev.* **1995,** *99*, 1727.
33. Ishikawa, K.; Uemori, T. *Phys. Rev. B* **1999,** *60*, 11841.
34. Schulmeyer, T.; Paniagua, S. A.; Veneman, P. A.; Jones, S. C.; Hotchkiss, P. J.; Mudalige, A.; Pemberton, J. E.; Marder, S. R.; Armstrong, N. R. *J. Mater. Chem.* **2007,** *17*, 4563.
35. Chiang, L.-Y.; Wang, L.-Y.; Kuo, C.-S. *Macromolecules* **1995,** *28*, 7574.
36. Chiang, L.-Y.; Wang, L.-Y.; Tseng, S.-M.; Wu, J.-S.; Hsieh, K.-H. *Synth. Met.* **1995,** *70*, 1477.